Journal of Power Sources 186 (2009) 417–427

Contents lists available at ScienceDirect

Journal of Power Sources

journal homepage: www.elsevier.com/locate/jpowsour

An improved one-dimensional membrane-electrode assembly model to predict the performance of solid oxide fuel cell including the limiting current density

Won Yong Lee, Daehyun Wee, Ahmed F. Ghoniem*

Department of Mechanical Engineering, Massachusetts Institute of Technology, Cambridge, MA 02139, USA

ARTICLE INFO

Article history:
Received 5 August 2008
Received in revised form 2 October 2008
Accepted 3 October 2008
Available online 15 October 2008

Keywords:
Solid oxide fuel cell
Membrane-electrode assembly
Dusty-gas model
Detailed electrode kinetics
Rate-limiting switchover

ABSTRACT

The limiting current density is an important characteristic quantity in solid oxide fuel cells (SOFCs). High concentration overpotential is often used to explain the limiting current density assuming a high tortuosity or limited surface diffusion in the vicinity of the three-phase boundary. Most membrane-electrode assembly models of SOFC fail to predict the limiting current density, even for hydrogen, when using physically reasonable values of tortuosity and considering the short residence time of the adsorbed species near the three-phase boundary. In this paper, a one-dimensional model for the transport–chemistry interactions in SOFCs is described. The model is based on a comprehensive approach that includes the dusty-gas model for gas transport in the porous electrodes, detailed heterogeneous elementary reaction kinetics for the thermo-chemistry in the anode, and detailed electrode kinetics for the electrochemistry. Correct values for the Knudsen diffusion coefficients are used. We apply the unsteady form of the conservation equations, allowing for the analysis of the response of the cell to external dynamics. Results of our model are compared with experimental data, showing good agreement over a wide range of the current density, but fail to predict the limiting current density accurately when the hydroxyl oxidation charge-transfer reaction is assumed to be the rate limiting reaction. To obtain accurate predictions of the limiting current density, we analyze the possibility that different steps can be rate-limiting reactions in the electrochemistry model of hydrogen oxidation. We use recent measurements on the three-phase boundary area and take into account the surface diffusion and competitive adsorption to determine possible rate limiting reactions at high current density. We show that a rate-limiting switchover model, in which the reaction limiting the overall kinetic rate becomes the hydrogen adsorption at the anode, may be required to explain the experimentally measured limiting current density over a range of operating conditions.

1. Introduction

Fuel cells are considered attractive alternatives to combustion engines because of their high theoretical efficiency. Solid oxide fuel cells (SOFCs) have special advantages over low temperature fuel cells such as polymer electrolyte membrane fuel cells because they exhibit high conversion efficiency at high temperatures while consuming hydrocarbons directly. Current SOFC research focus areas include reducing the operating temperature and eliminating the need for reformers while utilizing hydrocarbon fuels. In order to achieve these objectives while improving the finite current efficiency and optimizing the design of SOFCs, mathematical models are indispensable.

The limiting current density is an important characteristic quantity in SOFCs. Efforts to predict the limiting current density have not been successful. The high concentration overpotential, determined by the reactants and products transport limitations that reduce the reactants' concentrations at the three-phase boundary (TPB), is often used to explain the limiting current density. The concentration overpotential depends on the transport properties of the electrodes including their porosities and tortuosities. To predict the measured limiting current density, some membrane-electrode assembly (MEA) models assume anode tortuosities in the range of 10–17. These values are too high, considering that the reported range for porous sintered ceramics is 2–10, and most often below 6 [1]. To avoid making this assumption, Williford et al. [1] introduced surface diffusion effects into Fick's diffusion model, by adjusting the diffusion coefficients assuming that the competitive adsorption and surface diffusion contribute to the concentration overpotential. The adjusted diffusion coefficient was introduced by combining a gas diffusion coefficient and a surface diffusion coefficient, and was applied to the gas species transport throughout the entire thickness of electrodes. This approach overestimated the diffusion resistance because: (i) the diffusion coefficient adjusted using the surface

* Corresponding author. Tel.: +1 617 253 2295; fax: +1 617 253 5981.
E-mail address: ghoniem@mit.edu (A.F. Ghoniem).

0378-7753/$ – see front matter © 2008 Elsevier B.V. All rights reserved.
doi:10.1016/j.jpowsour.2008.10.009

diffusion coefficient is applied to the gas species transport; and (ii) the adjusted coefficient is applied to the whole electrode even though surface diffusion plays a role only in the vicinity of the TPB, within tens of nanometers.

In this paper, we propose other mechanisms that can explain the cell behavior around the limiting current density. For this purpose, we develop an accurate transport–chemistry interaction model for the MEA, using the dusty-gas model (DGM) to describe transport; a detailed mechanism for the thermochemistry in the anode; and multistep reaction mechanisms to model the charge-transfer reactions at the anode and the cathode surfaces. We show that the model can predict the polarization curve accurately over most of the range of current density, while using the assumption that hydroxyl ion oxidation reaction is the limiting step in the anode electrochemistry model. However, this assumption fails to predict the limiting current density accurately. We explore other rate limiting reactions at high current density and show that hydrogen adsorption at the anode can become sufficiently slow to cause rapid increase of the activation overpotential at high currents. Using a modified approach to the selection of the rate limiting reaction, we obtain better prediction of the limiting current density.

In the following sections, a detailed model to calculate each overpotential and the way to implement them in the simulation code will be described. We will validate the model against available experimental results and propose a new rate-limiting switch-over model to improve the prediction of the limiting current density. The paper ends with conclusions and suggestions for future work.

2. Model description

The objective of the model is to calculate the polarization curve of a SOFC over the entire operating range of voltage–current density, and for different fuel concentrations. We adopt a one-dimensional approach to model transport–chemistry interactions within the MEA and limit our validation to button cell results. Extension to multi-dimensional models will be attempted in the future. We assumed that the temperature is constant and uniform through the MEA.

The equilibrium potential, E_{rev}, is calculated from the Gibb's free energy of the reaction:

$$E_{rev} = -\frac{\Delta g^0}{zF} - \frac{RT}{zF}\ln\frac{\prod_{prod} p_i^{\nu_i}}{\prod_{react} p_i^{\nu_i}} \quad (1)$$

where ν_i is the stoichiometric coefficient of a constituent, $\Re$ is the universal gas constant ($J\,mol^{-1}\,K^{-1}$), T is the temperature (K), p_i is the partial pressure of gas species i (atm), and the Gibbs free energy of reaction, Δg^0 ($J\,mol^{-1}$) is evaluated for all species at atmospheric pressure. E_{rev} is also the open circuit voltage (OCV) with no fuel leakage.

At finite current, the open circuit voltage is reduced by losses, including the ohmic overpotential associated with ion transport through the electrolyte and electron transport through the electrodes, the activation overpotentials associated with the energy barriers of the charge-transfer reactions, and the concentration overpotentials associated with the gas-phase species transport resistance through the electrodes. Thus, the operating cell voltage, E, can be written as

$$E_{cell} = E_{rev} - \eta_{conc,a} - \eta_{a,a} - \eta_{ohm} - \eta_{conc,c} - \eta_{a,c} \quad (2)$$

where $\eta_{conc,a}$ and $\eta_{conc,c}$ are the concentration overpotentials at the anode and the cathode, $\eta_{a,a}$ and $\eta_{a,c}$ are the corresponding activation overpotentials at the anode and the cathode, and η_{ohm} is the total ohmic overpotential. Models for these overpotentials are developed next.

2.1. Concentration overpotential

At open-circuit conditions, i.e. zero current flow, the species concentrations at the TPB are the same as those of the bulk channel's gases. Under finite current conditions, species concentrations at the TPB are different, because of the finite transport flux across the electrodes. While evaluating the actual electrochemical potential of the fuel cell, the relevant reactants and products concentrations are those at the TPB. The potential difference associated with the gas species concentration change across the electrodes is the concentration overpotential:

$$\eta_{conc} = [E_{rev}]_{\text{at the channel}} - [E_{rev}]_{\text{at the TPB}} = -\frac{RT}{zF} \times \left[\left(\ln\frac{\prod_{prod} p_i^{\nu_i}}{\prod_{react} p_i^{\nu_i}}\right)_{\text{at the channel}} - \left(\ln\frac{\prod_{prod} p_i^{\nu_i}}{\prod_{react} p_i^{\nu_i}}\right)_{\text{at the TPB}}\right] \quad (3)$$

Next we develop a model for computing the concentrations of gas species at the TPB.

2.1.1. Conservation equation

The conservation equation of gas-phase species in the reactive porous media is

$$\frac{\partial c_k}{\partial t} = A_s \dot{s}_{surf,k} + \dot{s}_{gas,k} - \nabla \cdot J_k \quad (k = 1, \ldots, K_g) \quad (4)$$

where c_k is the concentration of gas species k ($mol\,m^{-3}$), J_k is the molar flux of gas species k ($mol\,m^{-2}\,s^{-1}$), $\dot{s}_{surf,k}$ is the surface production rates of the gas species k by the heterogeneous reactions ($mol\,m^{-2}\,s^{-1}$), A_s is the specific catalyst area per unit volume of the electrode (m^{-1}), $\dot{s}_{gas,k}$ is the production rates of the gas species k by the homogeneous reactions ($mol\,m^{-3}\,s^{-1}$), and K_g is the total number of gas species. The molar flux can be determined by the Fick's model (FM) or the DGM. The production rates of the gas species are obtained from the thermo-chemistry model.

The surface species conservation equation is as follows:

$$\frac{\partial c_{surf,k}}{\partial t} = \dot{s}_{surf,k} \quad (k = 1, \ldots, K_s) \quad (5)$$

where $c_{surf,k}$ is the concentration of surface species k ($mol\,m^{-2}$), $\dot{s}_k$ is the production rate of the surface species k by the heterogeneous reactions ($mol\,m^{-2}\,s^{-1}$), and K_s is the total number of surface species. Unlike gaseous species, surface species are effectively immobile on length scales larger than an individual catalyst particle. Hence, the surface species transport over macroscopic distance is assumed negligible [2].

2.1.2. Transport

The fluxes J_k are computed using the DGM [3]. DGM incorporate physical phenomena beyond those described by FM, such as osmotic diffusion, reverse diffusion, and diffusion barrier [4]:

$$-\nabla c_i = \sum_{j(\neq i)} \frac{1}{c_t D_{ij}^e}(c_j J_i - c_i J_j) + \frac{J_i}{D_{iM}^e} + \frac{B_0}{\mu_{mix}^{\nu}}\frac{c_i}{D_{iM}^e}\nabla p \quad (6)$$

where $c_t = p/\Re T$ is total molar concentration ($mol\,m^{-3}$).

The effective Knudsen diffusion coefficient for the component i, D_{iM}^e, in the multicomopnent mixture gas is governed by [3]:

$$D_{iM}^e = \frac{d_0}{3}\frac{\varepsilon}{\tau}\sqrt{\frac{8RT}{\pi M_i}} \quad (7)$$

where M_i is the molar mass of species i ($kg\,mol^{-1}$), D_{ij}^e, is the effective binary diffusion coefficient in the porous medium, and D_{ij}^e is

related to the corresponding ordinary binary diffusion coefficient D_{ij} as [4]:

$$D_{ij}^{e} = \frac{\varepsilon}{\tau} D_{ij} \tag{8}$$

where ε is the porosity and τ is the tortuosity. The porosity is defined as

$$\varepsilon = \frac{\forall_{void}}{\forall_{material}} \tag{9}$$

in which $\forall_{void}$ is a void volume and $\forall_{material}$ is the superficial volume of the material.

The tortuosity is defined as

$$\tau = \left(\frac{l^e}{l}\right)^2 \tag{10}$$

where l^e is the effective length between two points through the pores and l is the straight distance between the same two points.

According to Champan–Enskog kinetic theory, the binary diffusion coefficient D_{ij} is [5]:

$$D_{ij} = 5.8765 \times 10^{-9} \frac{\sqrt{T^3(1/M_i + 1/M_j)}}{P\sigma_{ij}^2 \Omega_{D,ij}} \tag{11}$$

where $\Omega_{D,ij}$ is the dimensionless collision integral function [5]:

$$\Omega_{D,ij} = fcn\left(\frac{k_B T}{\varepsilon_{ij}}\right) \tag{12}$$

where k_B is the Boltzmann constant ($J\,K^{-1}$) and ε_{ij} is the characteristic Lennard–Jones energy (J). Here, σ_{ij} and ε_{ij} are calculated from the individual parameters using the approximate equations [5]:

$$\sigma_{ij} = \frac{\sigma_i + \sigma_j}{2} \tag{13}$$

$$\varepsilon_{ij} = \sqrt{\varepsilon_i \varepsilon_j} \tag{14}$$

The mixture viscosity, μ_{mix}^{v}, is [5]:

$$\mu_{mix}^{v} = \sum_{i=1}^{n} \frac{X_i \mu_i^v}{\sum_{j=1}^{n} X_j \Phi_{ij}} \tag{15}$$

in which

$$\Phi_{ij} = \frac{1}{\sqrt{8}}\left(1 + \frac{M_i}{M_j}\right)^{-1/2}\left[1 + \left(\frac{\mu_i^v}{\mu_j^v}\right)^{1/2}\left(\frac{M_j}{M_i}\right)^{1/4}\right]^2 \tag{16}$$

The viscosity of each species is determined by [5]:

$$\mu^v = 8.4411 \times 10^{-5} \frac{\sqrt{MT}}{\sigma^2 \Omega_\mu} \tag{17}$$

in which

$$\Omega_\mu = fcn\left(\frac{k_B T}{\varepsilon}\right) \tag{18}$$

The permeability B_0 is an experimentally determined characteristic parameter of the porous matrix structure including the porosity and tortuosity factors. If an electrode is assumed to be an aggregated bed of spherical particles with diameter d_p (m), the permeability can be expressed by the Kozeny–Carman relationship [6]:

$$B_0 = \frac{d_p^2}{180} \frac{\varepsilon^3}{(1-\varepsilon)^2} \tag{19}$$

The transport of gaseous species through porous electrodes is affected by the microstructure of the electrodes, particularly, the porosity, permeability, pore size, and tortuosity factor.

2.1.3. Thermo-chemistry

Because of the relatively high operating temperatures and the catalytic surfaces in the anode structure, various thermochemical reactions occur within the anode, such as steam reforming, water–gas shift, partial oxidation, and carbon formation. Thermochemistry has usually been handled using significantly simplifying assumptions, such as local equilibration of reforming and water–gas-shift chemistry [1,7], or global reaction kinetics [8]. Recently, detailed heterogeneous elementary kinetics models of methane on a Ni surface have been established and validated over a wide range of conditions [9].

Gas-phase chemistry within the pores is neglected because the heterogeneous thermochemical reactions are considerably faster than the homogeneous thermochemistry and the probability for gas–gas collisions is low when the pore space is comparable to the mean free-path length [9]. Thus,

$$\dot{s}_{gas,k} = 0 \quad (k = 1, \ldots, K_g) \tag{20}$$

The surface mechanism of methane reforming and oxidation over nickel has been suggested [10]. The mechanism was initially developed and validated using Ni-coated honeycomb monoliths for the temperature range from 700 to 1300 K. The reaction mechanism consists of 6 pairs of adsorption/desorption reactions for 6 gas species and 15 pairs of surface reactions among 12 adsorbed species. We included all 44 heterogeneous elementary reactions in the model. Details on how to apply detailed thermochemical reforming to our model can be found in [11].

2.2. Activation overpotential

Charge-transfer processes are among the least understood aspects of fuel-cell chemistry. Analytical approaches using a single global charge-transfer reaction have often been used to describe electrochemical kinetics, leading to the Butler–Volmer equation [1,12,13]. There have been some efforts to develop detailed charge-transfer kinetics in the form of elementary reaction steps, in a manner that resembles the treatment of heterogeneous thermochemical kinetics. However, a clear understanding of the electrode kinetics does not exist yet. Regarding the anode, there are several outstanding issues. According to the literature, adsorption/desorption, surface diffusion, the formation of hydroxyl and a charge-transfer reaction are feasible rate-limiting reaction steps in a simplified SOFC anode model. It is not evident whether the chemical and the electrochemical reactions occur only on the surfaces of N_i and of yttria-stabilized zirconia (YSZ), or whether the bulk material is also active.

Zhu et al. [9] applied a detailed electrode kinetics model and obtained a Butler–Volmer formalism using a rate-limiting step. This approach provides qualitative information about some important functional dependencies such as the reaction order in the exchange current density, and enables comparison with experimental results that have been interpreted using parameters in the Butler–Volmer equation. In the following, we follow the same approach.

2.2.1. Anode activation overpotential

We use the five elementary reaction mechanisms proposed by de Boer [14]. In this model, hydrogen is adsorbed only on the nickel surface (Ni) and other surface species reside on the electrolyte surface (YSZ). These reactions include interactions among (i) an adsorbed atomic hydrogen, H(Ni), an empty surface site, (Ni), and an electron, e^-(Ni), on the Ni anode surface; (ii) a lattice oxygen, $O_O^\times$ (YSZ), and an oxygen vacancy, $V_O^{\bullet\bullet}$ (YSZ) within the YSZ electrolyte; and (iii) hydroxyl ion OH^-(YSZ), water H_2O(YSZ), oxygen ion O^{2-}(YSZ), and empty sites (YSZ) on the YSZ surface. The reaction mechanism is

Table 1
The different terms and parameters in BV equation when assuming that Reaction (R1), (R2), (R3) or (R4) is rate-limiting.

Rate-limiting reaction	Exchange current density	$i^*_{H_2}$	β_a	β_c
1	$i_0 = i^*_{H_2}(p_{H_2})$	$2Fl_{TPB}\frac{S^0_i}{\sqrt{2\pi\Re TM_{H_2}}}$	0	2
2	$i_0 = i^*_{H_2}\frac{p^{1/4}_{H_2O}(K_1p_{H_2})^{1/4}}{1+(K_1p_{H_2})^{1/2}}$	$\frac{2l_{TPB}FK^{1/4}_5k^{3/4}_{2,a}k^{1/4}_{2,c}}{(K_3K_4)^{1/4}}$	0.5	1.5
3	$i_0 = i^*_{H_2}\frac{(K_1p_{H_2})^{1/4}(p_{H_2O})^{3/4}}{1+(K_1p_{H_2})^{1/2}}$	$2l_{TPB}Fk_{3,c}(K_3K_2)^{1/4}\left(\frac{K_5}{K_4}\right)^{3/4}$	1.5	0.5
4	$i_0 = i^*_{H_2}(p_{H_2O})$	$2Fl_{TPB}k_{4b}K_5$	2	0

- Adsorption on the Ni surface:

$$H_2(g) + 2(Ni) \Leftrightarrow 2H(Ni) \quad (R1)$$

- Charge-transfer reactions at the TPB region:

$$H(Ni) + O^{2-}(YSZ) \Leftrightarrow (Ni) + OH^-(YSZ) + e^-(Ni) \quad (R2)$$

$$H(Ni) + OH^-(YSZ) \Leftrightarrow (Ni) + H_2O(YSZ) + e^-(Ni) \quad (R3)$$

- Adsorption/desorption on the YSZ surface:

$$H_2O(YSZ) \Leftrightarrow H_2O(g) + (YSZ) \quad (R4)$$

- Transfer of oxygen ion between the surface and the bulk YSZ:

$$O^X_0(YSZ) + (YSZ) \Leftrightarrow O^{2-}(YSZ) + V_O^{\bullet\bullet}(YSZ) \quad (R5)$$

The calculated residence time of H on Ni surface is 8 ns and the corresponding diffusion length is 19 nm at 750 °C. Because the adsorbed hydrogen desorbs after this small diffusion length, the surface coverage is mainly determined by adsorption/desorption. Even within the diffusion length scale, 50 nm, away from the TPB the surface coverage changes by only 0.1%. Thus, it is reasonable to exclude the surface diffusion of hydrogen from this mechanism.

The surface species interact through five reaction equations, Reactions (R1)–(R5) and the two conservation equations for Ni and YSZ surface. Invoking the assumption that one reaction step is rate-limiting, a simple analytical expression for the i–η_a relationship can be derived in the Butler–Volmer form (BV) using the anodic and the cathodic reaction coefficient, $k_{i,a}$ and $k_{i,c}$ of the rate-limiting reaction and the equilibrium constants K_i of other reactions. The form of the BV equation is

$$i = i_0\left[\exp\left(\beta_a\frac{F\eta_a}{RT}\right) - \exp\left(-\beta_c\frac{F\eta_a}{RT}\right)\right] \quad (21)$$

where β_a and β_c are the anodic and cathodic charge-transfer coefficient, respectively. The results of these derivations, assuming that Reaction (R1), (R2), (R3) or (R4) may be the rate limiting reaction, are shown in Table 1. Note that different expressions are obtained for the exchange current density, their dependence on the partial pressure of the reactants and product, and the charge-transfer coefficients. The form of these expressions are important in determining the actual rate limiting reaction under different operating conditions, as shown next.

Zhu et al. [9] derived the BV type i–η_a relationship assuming that Reaction (R3) is rate-limiting, and used that expression in their modeling analysis. They based their choice on the argument that the hydrogen adsorption rate is several orders of magnitude higher than the current density of interest [15,16] and hence cannot be rate-limiting. In the following we show that this is indeed a good choice for the rate limiting reaction over a wide range of current density, but not necessarily at high current density.

We analyzed the possibilities that reactions other than Reaction (R3) can be rate-limiting, especially at high current density, and examined the possibility that hydrogen adsorption Reaction (R1) may be the rate-limiting. For this purpose, we need to show that other reaction rates match the expected values of the current density. In the following, we calculate the hydrogen adsorption rate based on the estimate of the TPB area using recent 3D reconstruction of the anode/electrolyte interface.

(a) TPB area:

Recently, a 3D reconstruction of the anode was obtained by stacking the 2D scanning electron microscopy (SEM) images in 3D space. From the 3D reconstruction, the volume-specific TBP length was directly determined. It was found to be 4.28×10^{12} m^{-2}. For the electrochemical reactions to take place, the TPB must be connected to the rest of the structure. That is, the pores must be connected through the surrounding pore network to the fuel stream, the Ni phase connected to the surrounding Ni phase then ultimately to the current collector, and the YSZ phase connected to the bulk YSZ electrolyte. It is reported that 63% of TPBs were interconnected [17]. Moreover, it was argued that the TPB width is in the range of 10^{-9}–10^{-10} m in [18] and 5×10^{-10} m in [1]. The active depth of the anode is O(10 μm) [19]. Based on these values, the TPB area per electrode area can be calculated as follows:

$$\frac{A_{TPB}}{A_{electrode}} = 0.63\times(4.28\times10^{12})\times(10\times10^{-6})\times(5\times10^{-10}) = 0.013 \quad (22)$$

(b) Hydrogen adsorption rate at the TPB:

Using the sticking coefficient of hydrogen on nickel, the hydrogen adsorption rate can be computed from the following expression [20]:

$$R_1 = 10^{-2}\sqrt{\frac{\Re T}{2\pi M_{H_2}}}c_{H_2}\theta_v^2 \quad (23)$$

where θ_v is a vacancy coverage.

The concentration of hydrogen in the gas channel is in the order of several mol m^{-3}. If all the adsorbed hydrogen reacts, the order of magnitude of the resulting current density is as follows:

$$i = \frac{A_{TPB}}{A_{electrode}}\times F\times R_1 \sim O\ (1\,A\,cm^{-2}) \quad (24)$$

This result shows that the hydrogen adsorption rate and the current density of interest are indeed comparable. Thus, at high current density, hydrogen adsorption at the anode may be the rate limiting reaction. We should mention, however, that the current density estimated in Eq. (24), based on the TPB area and the adsorption rate of hydrogen on this area, may be too high. For instance, since A_{TPB} is the combined area of nickel and YSZ surfaces, the actual area of Ni surface for hydrogen adsorption may be smaller than the value given in Eq. (22). Furthermore, the present model assumes that only hydrogen can be adsorbed on the nickel surfaces. However, other species such as H_2, H_2O, OH, and O can also be adsorbed on nickel surfaces [1]. Considering the actual available Ni surface area of the TPB for hydrogen adsorption, and the competitive

adsorption of other species, we conclude that the hydrogen adsorption rate, under the condition of high current, can be the rate-limiting reaction. Thus, the case when Reaction (R1) is rate-limiting at high current density is included in our analysis. As shown next, other considerations must be taken into account in defining the rate limiting reaction.

Determining the actual rate limiting reaction among Reactions (R1)–(R4), requires careful analysis, which is based on several observations and/or matching the form of the corresponding Butler–Volmer equation to experimental data. Experimental results have shown a number of trends that are relevant to the anode charge-transfer reaction.

(1) The anodic charge-transfer coefficient, β_a, is greater than the value often assumed when a single rate-limiting charge-transfer reaction is used over the entire range of current density; that is, it is greater than 0.5.
(2) It has been reported that small amounts of water added to the fuel gas accelerates the electrochemical charge-transfer reaction, known as the catalytic effect of water [14,16,21]. Considering the global reaction in the anode, the partial pressure of hydrogen, a reactant, is expected to have a positive reaction order, while the partial pressure of water, a product, is expected to have a negative reaction order. This is, however, contrary to what is observed experimentally; as it is, water promotes the electrochemical reactions.

If Reaction (R3) or (R4) is assumed to be the rate-limiting process:

(i) the anodic charge-transfer coefficient in the BV becomes 1.5 or 2, respectively, when anodic and cathodic charge-transfer coefficients of the elementary charge-transfer steps are assumed to be 0.5, and
(ii) the reaction order of water in the exchange current density becomes positive.

Thus, either reaction could be rate limiting and compatible with the above observation. However, there is a distinction. If Reaction (R4) is assumed to be the rate-limiting reaction, the exchange current density does not depend on the hydrogen concentration and the cathodic charge-transfer coefficient reduces to zero. According to de Boer, the anodic charge-transfer coefficient in most cases was close to 1.5 for cermet anode. For the cathodic branch, the charge-transfer coefficient is approximately 0.5–1.0. Furthermore, for Ni patterned anodes, a considerable influence was found for p_{H_2} on the polarization resistance, especially at a very low partial pressure of hydrogen [21]. Thus, we conclude that the analytic expression of the Butler–Volmer form exhibits a better agreement with experiments when Reaction (R3) rather than Reaction (R4) is assumed to be the rate-liming reaction.

2.2.2. Cathode activation overpotential

The overall oxygen reduction and incorporation at the electrode–electrolyte interface can be written as

$$\tfrac{1}{2}O_2(g) + V_O^{\bullet\bullet}(el) + 2e^-(c) \leftrightarrow O_0^X(el)$$

where $V_O^{\bullet\bullet}$(el) and $O_0^X(el)$ denote the oxygen vacancies and lattice oxygen ions in the bulk of the electrolyte and $e^-(c)$ are the electrons within the cathode. As with the oxidation of hydrogen at the anode, the global reaction is the result of elementary steps. Here, it is assumed that oxygen reduction proceeds in two steps [9]:

- Adsorption/desorption:

$$O_2(g) + 2(c) \Leftrightarrow 2O_{ad}(c) \quad \text{(R6)}$$

- Charge-transfer and incorporation at the TPB:

$$O_{ad}(c) + V_O^{\bullet\bullet}(el) + 2e^-(c) \Leftrightarrow O_0^X(el) + (c) \quad \text{(R7)}$$

In these reactions $O_{ad}(c)$ is the adsorbed atomic oxygen on the cathode surface and (c) is an unoccupied cathode surface site.

Assuming that the charge-transfer coefficients are 0.5, the BV form of i-relationship simplifies to

$$i = i_0\left(\exp\left(\frac{F\eta_a}{2\Re T}\right) - \exp\left(-\frac{F\eta_a}{2\Re T}\right)\right) \quad (25)$$

$$i_0 = \frac{2l_{TPB}Fk_{7,c}^{1/2}k_{7,a}^{1/2}(p_{O_2}K_6)^{1/4}}{(K_6^{1/2} + p_{O_2}^{1/2})} \quad (26)$$

By writing

$$i_{O_2}^* = 2l_{TPB}Fk_{7,c}^{1/2}k_{7,a}^{1/2} \quad (27)$$

the exchange current density is expressed as

$$i_0 = i_{O_2}^* \frac{(p_{O_2}/K_6)^{1/4}}{1 + (p_{O_2}/K_6)^{1/2}} \quad (28)$$

For an LSM–YSZ interface, K_6 is represented in Arrhenius form [22]:

$$K_6 = A_{O_2}\exp\left(\frac{E_{O_2}}{\Re T}\right) \quad (29)$$

in which $A_{O_2} = 4.9 \times 10^8$ atm and $E_{O_2} = 200$ kJ/mol.

Even though there is a discrepancy in the exponent of oxygen partial pressure in the numerator, Eq. (28) matches well the experimental results given by [22]:

$$i_0 = i_{O_2}^* \frac{(p_{O_2})^{1/2}}{1 + (p_{O_2}/K_6)^{1/2}} \quad (30)$$

The parameter $i_{O_2}^*$ is taken here as an adjustable parameter that is varied to match the experimentally observed cell performance reported by Jiang and Virkar [7] under one set of conditions. It is then used unchanged to predict the cell performance under other conditions.

2.3. Ohmic overpotential

Sources of ohmic losses in a fuel cell are the ion flow resistance across the electrolyte and the electronic flow resistance across the electrode. The electrolyte has several order-of-magnitude higher resistivity than the electrodes and the interconnect. Thus, in an SOFC, the ohmic polarization is typically dominated by ion resistance thorough the electrolyte. The ohmic overpotential can be expressed as [23]:

$$\eta_{ohm} = i_e R_{el} \quad (31)$$

$$R_{el} = \frac{l_{el}}{\sigma_{el}} = (\Omega\,\mathrm{cm}^2) \quad (32)$$

$$\sigma_{el} = \sigma_0 T^{-1}\exp\left(-\frac{E_{el}}{RT}\right) = (\mathrm{S\,cm}^{-1}) \quad (33)$$

3. Simulation procedure

The model described in Section 2 is used to determine the cell voltage for a given current density, from zero current to the limiting current. The cell potential is expressed as the difference between the equilibrium potential E_{rev} and the sum of all the relevant overpotentials, which depend on the current density.

The solution proceeds as follows.

(1) We calculate the equilibrium potential based on the global electrochemical reaction at zero current.
The equilibrium potential depends on the fuel and oxidant compositions in the corresponding channels, temperature and pressure.

(2) We calculate the concentration overpotentials.
- First we set up the boundary conditions:
The boundary conditions at the channel–electrode interface are established by requiring the gas-phase species concentrations to match those in the gas channel. At the anode/electrolyte interface, the boundary condition of each gas species depends on the charge-transfer chemistry, and hence the current density.

$$J_k = \nu_k \frac{i}{zF} \tag{34}$$

- We calculate the molar flux, J_k using the current values of the concentrations by substituting in the DGM, which is rearranged in the matrix form as follows:

$$-\nabla c_i - \frac{B_0}{\mu^v_{mix}} \frac{c_i}{D^e_{iM}} \nabla P = \sum_{j(\neq i)} \frac{1}{c_t D^e_{ij}} (c_j J_i - c_i J_j) + \frac{J_i}{D^e_{iM}} = [H][J] \tag{35}$$

where $[J]$ is a flux column vector and $[H]$ matrix is defined as

$$h_{kl} = \left[\frac{1}{D^e_{kM}} + \sum_{j \neq k} \frac{X_j}{D^e_{kj}} \right] \delta_{kl} + (\delta_{kl} - 1) \frac{X_k}{D^e_{kl}} \tag{36}$$

Because the pressure is determined using the ideal gas law, the left hand side of Eq. (35) is calculated from the present values of the concentrations of gas species and the concentration boundary conditions at the channel, estimating ∇c_i using forward difference approximation. The matrix $[H]$ in the right hand side of Eq. (35) is expressed in terms of the diffusion coefficients and the mole fractions in Eq. (36) and calculated in the same way. Hence, the molar flux can be calculated as

$$[J] = [H]^{-1}[LHS] \tag{37}$$

We then substitute J_k in the following conservation equation of the gas species:

$$\frac{\partial c_k}{\partial t} = A_s \dot{s}_{surf,k} - \nabla \cdot J_k \quad (k = 1, \ldots, K_g) \tag{38}$$

$$\frac{\partial c_{surf,k}}{\partial t} = \dot{s}_{surf,k} \quad (k = 1, \ldots, K_s) \tag{39}$$

The conservation equations, Eq. (38) and (39), become a set of ordinary differential equations when Eq. (37) is cast into a finite-volume form using the flux boundary conditions at the interface. The electrodes are approximated as continuous media, with homogenized, volume averaged properties.

- We calculate $\dot{s}_k$ using the heterogeneous thermochemistry model based on the current values of the concentrations of the gas and surface species.
The ODEs of the gas species and surface species are solved simultaneously using 'ode15s' function in MATLAB® with the Gear's method option on.
- We calculate the concentrations at the interface between the electrodes and the electrolyte when the solution reaches steady state.
- We calculate the concentration overpotentials for each electrode, $\eta_{con,a}$ and $\eta_{con,c}$.

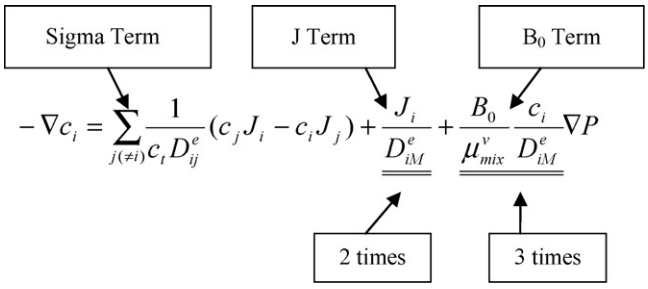

Fig. 1. Terms in the DGM that have been modified and the impact of the changes in the coefficient on the contribution of the corresponding terms to the concentration gradient.

(3) We calculate the activation overpotentials for each electrode:
The activation overpotentials, $\eta_{a,a}$ and $\eta_{a,c}$, are computed from BV type i–V relations for the anode and cathode, respectively. $\eta_{a,a}$ and $\eta_{a,c}$ are determined from the nonlinear solver function, 'fsolve' function in MATLAB®.

(4) The ohmic overpotential is calculated using Eq. (33).

(5) The cell voltage is calculated using Eq. (2).

4. Simulation results

Among the numerous 1D MEA models developed to describe the transport–chemistry interaction within the different elements, the model of Zhu et al. [9] is the most detailed one. Our model, while using the same equations, modifies the transport and activation overpotential models to improve their accuracy, as shown below. In order to evaluate the effect of each improvement, we compute i–V curve using a single rate-limiting reaction mode across the entire current density range, similar to that used in Zhu et al. [9]. Thus, Reaction (R3) is assumed to be the rate-limiting reaction over the entire range of current density. The button-cell experimental results by Jiang and Virkar [7] are used to establish the empirical parameters, $i^*_{H_2}$ and $i^*_{O_2}$, in the electrochemistry model by fitting the MEA experimental performance when mixtures of hydrogen and steam are fed to the anode. First, we demonstrate the limitation of this model, even after modifying the transport coefficients. Next, we use two different reactions as rate-limiting reactions, Reaction (R3) at low current density and Reaction (R1) at high current density, and show that this model predicts the limiting current density more accurately.

4.1. Model with a single rate-limiting reaction

First, we investigated the impact of the corrected transport coefficients, and compared the results with those obtained in [9]. We corrected the effective Knudsen diffusion coefficient based on [3] and adopted the permeability reported in [6]. The effective Knudsen diffusion coefficient used in [9] is a factor of 2 larger than reported in [3]. Furthermore, the permeability used in [9] is smaller than the permeability calculated using the Carman–Kozeny model shown in Eq. (19) by a factor equal to 0.4τ.

The values of the corresponding terms impacted by these coefficients are two to three times larger than those reported in [9], based on a tortuosity of 3.5. Each term that has been modified in our model is underlined in Fig. 1 and the approximate influence of each term is shown in the boxes below the term.

To assess the impact of the corrected Knudsen diffusion coefficient and the permeability in the DGM model, the same fuel cell used in [9] is modeled with the same fitting parameters in Table 2 reported in that paper.

Table 2
Simulation parameters.

Parameters	Value	Units
Parameters for an SOFC MEA structure		
Anode		
Thickness (l_a)	1220	μm
Porosity (ε)	0.35	
Tortuosity (τ)	3.50	
Average pore diameter (d_0)	1.00	μm
Average particle diameter (d_p)	2.50	μm
Specific catalyst area (A_s)	1080	cm^{-1}
$i^*_{H_2}$ (Reaction (R3) is rate-limiting)	8.5	$A\,cm^{-2}\,atm^{-3/4}$
$i^*_{H_2}$ (Reaction (R1) is rate-limiting)	15.963	$A\,cm^{-2}\,atm^{-1}$
Cathode		
Thickness (l_c)	30	μm
Porosity (ε)	0.35	
Tortuosity (τ)	3.50	
Average pore diameter (d_0)	1.00	μm
Average particle diameter (d_p)	2.50	μm
$i^*_{O_2}$	2.8	$A\,cm^{-2}\,atm^{-1/2}$
Electrolyte		
Thickness (l_{el})	25	μm
Activation energy of O^{2-} (E_{el})	8.0×10^4	$J\,mol^{-1}$
Pre-factor of O^{2-} (σ_0)	3.6×10^5	$S\,cm^{-1}$
Operating conditions		
Pressure	1	atm
Temperature	1073	K

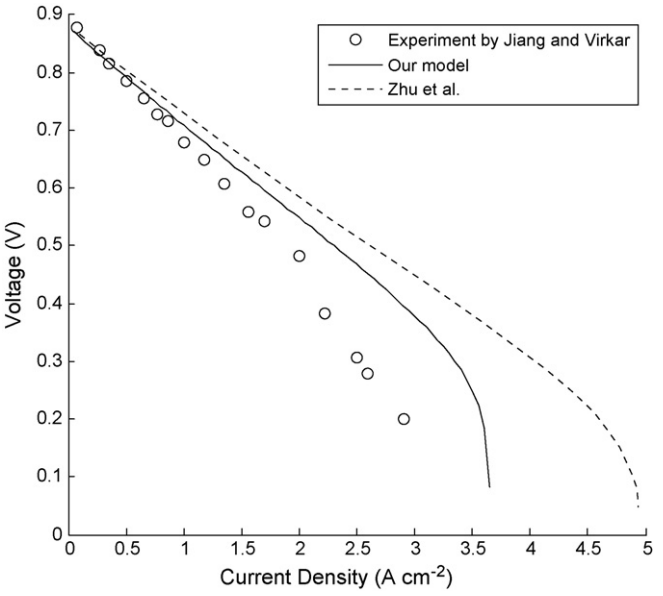

Fig. 3. Comparison between the experimental data [7] results shown by a continuous line, our model results shown by open circles and Zhu et al. [9] model results shown by a broken line when the anode stream is 50% H_2 + 50% H_2O.

Fig. 2 shows substantial difference between our model predictions using the corrected coefficients and those reported in [9], especially at the higher current density when the concentration overpotential is most relevant. For three different fuel concentrations at the anode, our model reaches the limiting current density faster than that reported in [9], and the difference is larger for higher fuel concentrations.

These results can be explained as follows. As the current density increases, the molar flux and the pressure gradient become larger leading to higher values of the magnitudes of the J term and the B_0 term in Fig. 1, making the impact of the two coefficients more important. When we calculated the J term and B_0 term while changing the current density from 0.2 to 3 $A\,cm^{-2}$ for the case where the hydrogen composition is 50%, the values of these two terms were found to increase by an order of magnitude. Most of the difference between our model results and those reported in [9] comes from the J term which includes the Knudsen diffusion coefficient. On the other hand, the B_0 term is not as significant because the permeability is small, $O(10^{-15})$, even though pressure gradient is high, $O(10^6)$.

Figs. 3 and 4 show that correcting the transport parameters leads to a better match with the experimental results of Jiang and Virkar [7]. However, even with these corrections, the model fails to accurately predict the value of the limiting current density. In the next section, we show that using a different reaction step at high current densities can further improve the model prediction.

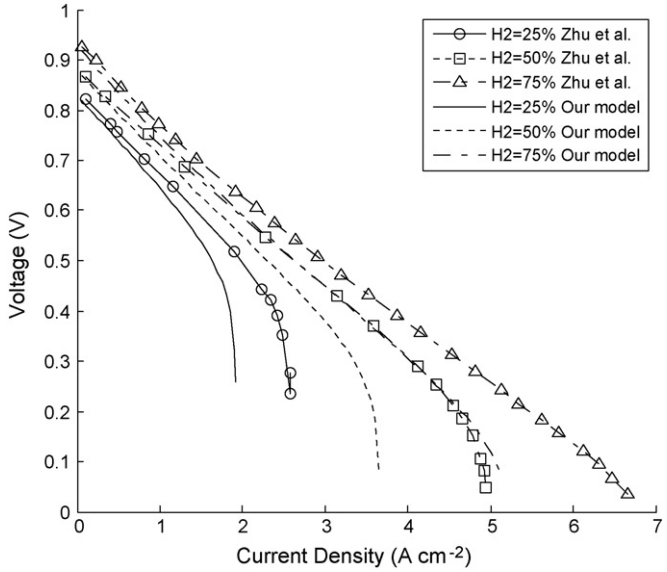

Fig. 2. Comparison between the polarization curves computed using our model and those reported in [9].

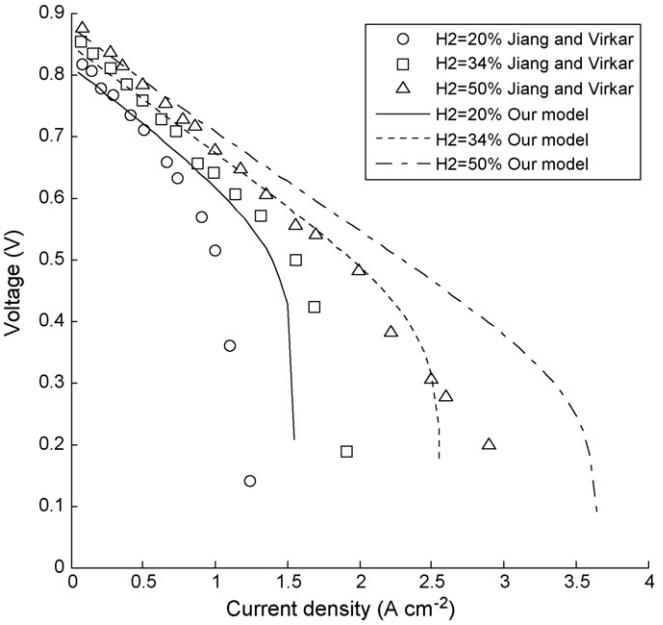

Fig. 4. Comparison between our model results, shown by lines, and experimental results of Jiang and Virkar [7], shown by open circles, rectangles, and triangles.

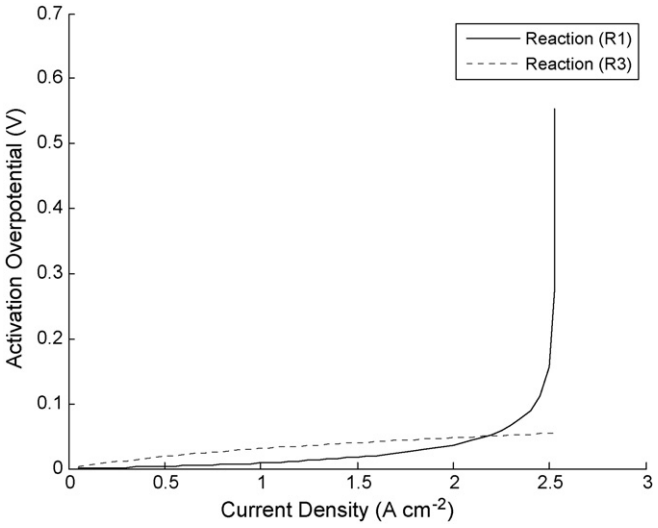

Fig. 5. The anode activation overpotential; the continuous line corresponds to the case when Reaction (R1) is rate-limiting and the broken line corresponds to the case when Reaction (R3) is rate-limiting while the anode stream is 50% H_2 + 50% H_2O.

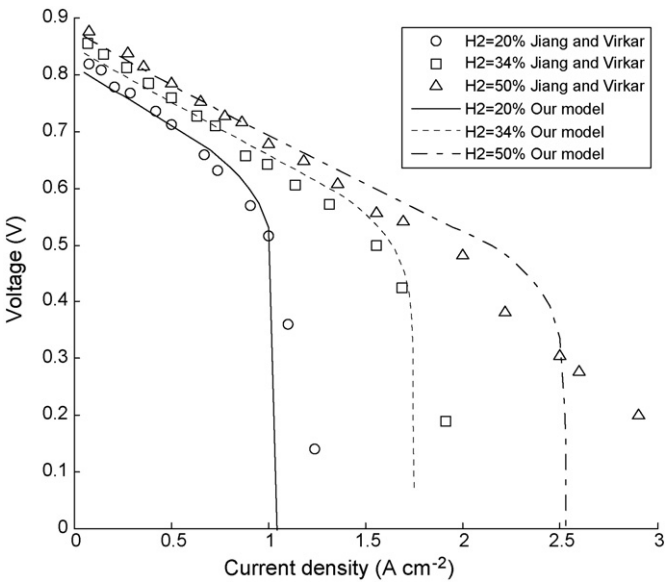

Fig. 6. Comparison between our model and experimental results by Jiang and Virkar [7].

4.2. Model with the rate-limiting reaction switch-over

Arguments, shown in Section 2.2.1, supporting the use of Reaction (R3) as the rate-limiting reaction may not be valid near the limiting current density. It has been claimed, based on experimental results in [16,21], that the adsorption of hydrogen at the anode may be rate-limiting process. We have also presented arguments to the effect that hydrogen adsorption can be the rate-limiting reaction under the condition of high current density. At high current density, a vast amount of water is produced and may compete against hydrogen for adsorption sites, reducing hydrogen adsorption rate [1]. Therefore, we propose a new model in which the rate-limiting reaction switches from the hydroxyl oxidation charge-transfer reaction, Reaction (R3), to the hydrogen adsorption reaction, Reaction (R1), near the limiting current density.

Fig. 5 shows the anode activation overpotential when Reaction (R1) or (R3) is assumed to be the rate-limiting reaction over the entire range of current density. Results show that at lower current densities, Reaction (R3) overpotential is indeed the larger value because it is the more sluggish reaction. However, as the current density increases, the concentration of hydrogen at the interface decreases resulting in the reduction of the exchange current density and Reaction (R1) overpotential rises sharply. This is consistent with the form of the BV equations shown in Table 1: the power of the hydrogen concentration in i_0 is 1 when Reaction (R1) is assumed to be the rate-limiting reaction, while it is 1/4 when Reaction (R3) is assumed to be the rate-limiting reaction. When hydrogen adsorption is rate-limiting, the anode activation overpotential soars as the exchange current density decreases because of the drop in hydrogen concentration.

In the following calculation, we use the point of intersection of the two curves in Fig. 5 as the switch-over point between two reactions, that is, the point at which we assume that Reaction (R3) is no longer the rate-limiting reaction, and instead Reaction (R1) is the rate-limiting reaction.

Results of our extended model are shown in Fig. 6. The results of the extended model agree better with the experimental measurements, although the limiting current density is now slightly under predicted, especially in the case of higher hydrogen concentration. This can be explained as follows. When Reaction (R1) was assumed to be the rate-limiting reaction, the numerical value of $i^*_{H_2}$ in Table 1 was obtained by fitting the experimental results for the case of 34% H_2 in the anode stream (and 66% H_2O). This value of $i^*_{H_2}$ was then assumed to be independent of the hydrogen concentration and was used in all the other cases, i.e. for 20% and 50% H_2 in the anode stream. Note that $i^*_{H_2} p_{H_2}$ is the hydrogen adsorption rate. Assuming that $i^*_{H_2}$ is constant is consistent with the assumption in Section 2.2.1 that only hydrogen can adsorb on the Ni surface. However, when we consider the competitive adsorption on the Ni surface, the TPB may be covered with more water molecules when the water concentration in the anode stream is higher. Thus, $i^*_{H_2}$ may depend on the concentration of H_2O and its value may be higher, instead of being constant, when there is 50% H_2O in the anode stream than when there is 66% H_2O. In other words, the activation overpotential may be over predicted in the case of 50% H_2 when the value of $i^*_{H_2}$ is estimated using the experimental data with 34% H_2. This explains why the limiting current density is slightly under predicted in Fig. 6 when the anode stream is 50% H_2.

When the hydrogen adsorption at the anode is taken to be the rate-limiting reaction, the exchange current density corresponds directly to the current density of the cell if all the adsorbed hydrogen is consumed in the electrochemical reaction, as shown in Table 1. In other words, the exchange current density is the maximum possible current density when the hydrogen adsorption reaction is rate-limiting. This is consistent with the i–$\eta_{act,a}$ relationship when Reaction (R1) is assumed to be rate-limiting:

$$i = i_0 \left[1 - \exp\left(-\frac{2F\eta_{act,a}}{RT}\right)\right] \tag{40}$$

As shown in Eq. (40), a significantly higher activation overpotential is required to support a current density close to the exchange current density. Therefore, the limiting current density is very close to the exchange current density.

Table 3
Rate-limiting switch-over point.

Hydrogen composition	i_{limit} (A cm^{-2})	i_{switch} (A cm^{-2}) @ $i_0/i = 1.67$	i_{switch}/i_{limit}
50%	2.5273	2.02	0.79
34%	1.7465	1.40	0.80
20%	1.05	0.85	0.81

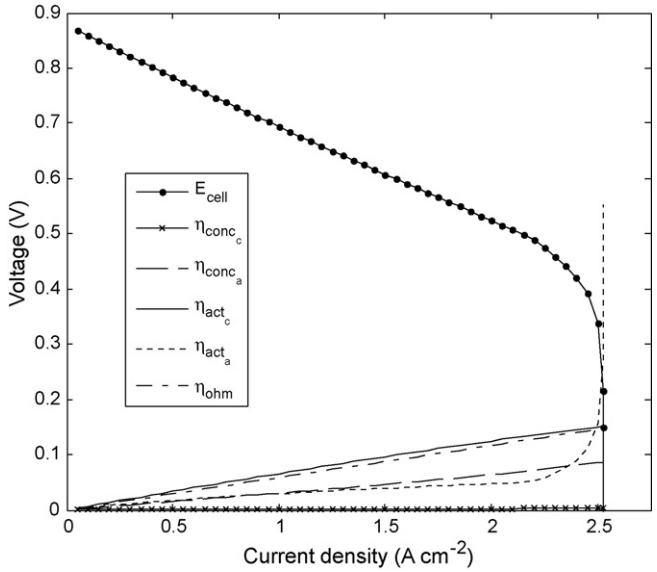

Fig. 7. The contributions of the five overpotentials when the anode stream is 50% H_2 + 50% H_2O.

Table 3 shows the computed limiting current density, $i_{\lim it}$, and the switching current density, i_{switch}, that is the current density at which we switch between Reactions (R1) and (R3). Results show that $i_{switch} = 0.6i_0$. Calculations in Table 3 show that the switching current density is nearly 80% of the limiting current density.

We conclude this section by restating the result of using different reactions as rate-limiting in different ranges of the current density. When the hydrogen adsorption rate is sufficiently fast to support the current density, such as 1.67 times the current density, the anode activation overpotential is determined by Reaction (R3). As the current density increases and the corresponding hydrogen adsorption rate decreases below this level, the rate-limiting reaction switches to Reaction (R1). In this regime, the anode activation overpotential rises abruptly with the current density and the electrochemical reaction proceeds very slowly until it is no longer possible.

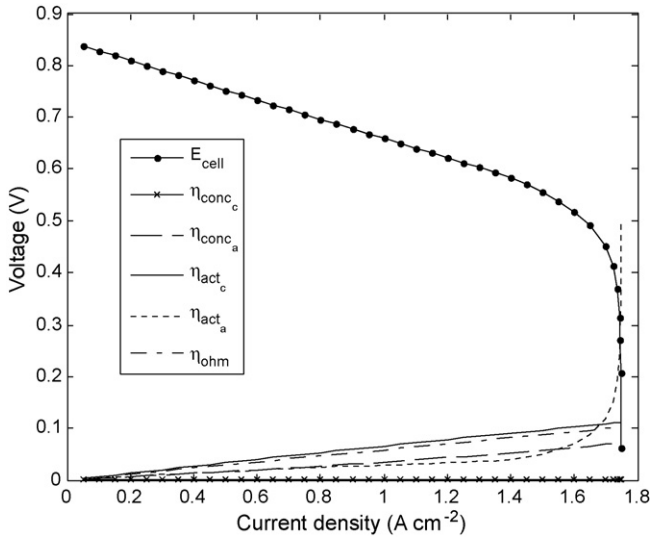

Fig. 8. The contributions of the five overpotentials when the anode stream is 34% H_2 + 66% H_2O.

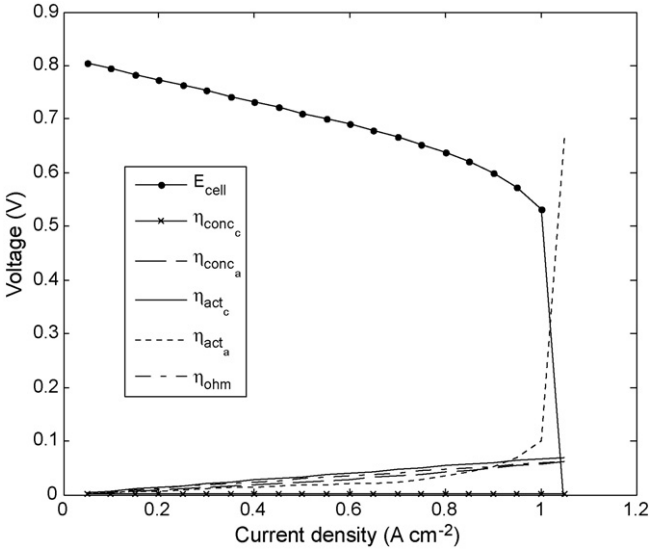

Fig. 9. The contributions of the five overpotentials when the anode stream is 20% H_2 + 80% H_2O.

4.3. Contribution of each overpotential

Figs. 7–9 show the contributions of each overpotential when the hydrogen concentration at the anode gas channel is 50%, 34%, and 20%, respectively. When the hydrogen composition is 50% or 34%, the ohmic overpotential and the cathode activation overpotential have almost the same magnitude, which is twice as large as the anode concentration overpotential. They are also more than twice as large as the anode activation overpotential, except near the limiting current density where anode activation overpotential is significant. When the fuel composition is 20% H_2, all overpotentials, except the cathode concentration overpotential, have nearly the same magnitude in the region away from the limiting current density. For all cases, as expected, the cathode concentration overpotential is negligible.

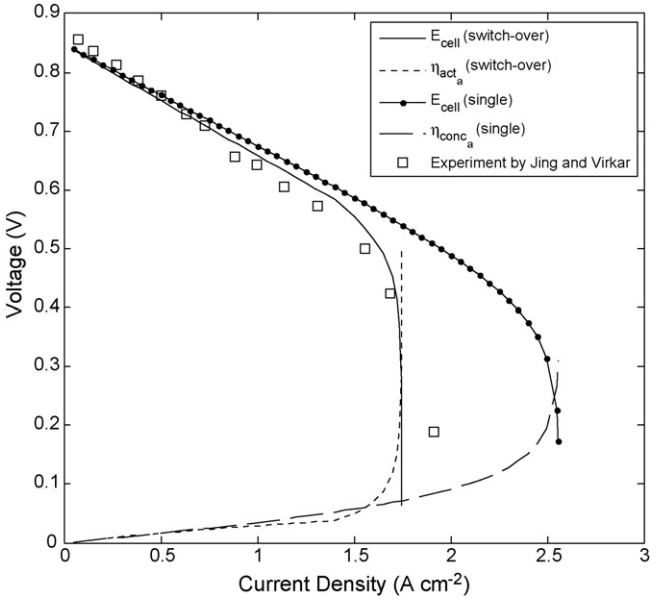

Fig. 10. Comparison between the experimental results by Jiang and Virkar [7] and the calculated operating cell voltages corresponding to the single rate-limiting reaction mode and the rate-limiting reaction switch-over mode, respectively, when the anode stream is 34% H_2 + 64% H_2O.

Table 4
The hydrogen concentrations at the channel, and the limiting current densities and the corresponding hydrogen concentrations at the interface for the single rate-limiting reaction mode and the rate-limiting reaction switch-over mode.

Channel		Single rate-limiting		Rate-limiting switch-over	
Mole fraction (%)	Concentration ($mol\,m^{-3}$)	Limiting current density ($A\,cm^{-2}$)	Concentration @ interface ($mol\,m^{-3}$)	Limiting current density ($A\,cm^{-2}$)	Concentration @ interface ($mol\,m^{-3}$)
20	2.17	1.55	0.002	1.05	0.738
34	3.74	2.56	0.002	1.75	1.256
50	5.53	3.65	0.017	2.03	1.817

For all known hydrogen/oxygen fuel cells, regardless of electrolyte type, it is believed that electrochemical reactions at the cathode are rate limiting and the activation overpotential is almost entirely due to cathode [24]. This is because hydrogen electrooxidation is extremely rapid on a wide range of catalysts. However, our results show that the ohmic overpotential has the same magnitude as the cathode activation overpotential. The ohmic overpotential is dominated by the ionic resistance in the electrolyte, which is a thermally activated vacancy hopping mechanism. The relatively lower operating temperature of 800 °C might explain these results. As we expect, the cathode activation overpotential is larger than the anode activation overpotential.

However, we also see that the electrochemical reaction cannot be sustained near the limiting current density because of the anode activation overpotential. It is often assumed that the concentration overpotential captures the impact of transport and the activation overpotential accounts for electrochemistry. Thus, it has been argued that the limiting current density occurs because of transport limitation, and the limiting current density has been explained using the rapid increase of the concentration overpotential. However, the activation overpotential also reflects the impact of the transport since the exchange current density depends on the concentrations. Fig. 10 shows a comparison between the experimental results by Jiang and Virkar [7] and the calculated operating cell voltages using the single rate-limiting reaction mode and the rate-limiting reaction switch-over mode, with their corresponding dominant overpotential. For the single rate-limiting mode, the limiting current density is governed by the rapid increase in the concentration overpotential when the hydrogen concentration at the interface approaches almost zero, as shown in Table 4. In the rate-limiting reaction switch-over mode, the sharp increase in the activation overpotential occurs before the rapid increase in the concentration overpotential. The hydrogen concentrations at the interface are not low enough to force the rapid increase in the concentration overpotential, as shown Table 4. However, the current density is close enough to the exchange current density to cause a sharp increase in the activation overpotential. Hence, the limiting current density is governed mainly by the activation overpotential rather than the concentration overpotential.

5. Conclusions

The model presented in this paper, which is similar in construction to the model presented in [9], is based on the DGM, detailed heterogeneous thermo-chemistry models, and detailed electrode kinetics models. We corrected the effective Knudsen diffusion coefficient and the permeability values, and showed improved predictive accuracy. We additionally analyzed the possibilities that a different intermediate step in the hydrogen electrochemical oxidation model is rate-limiting and proposed the rate-limiting switch-over model. The new model substantially improves the prediction of the limiting current density and shows better match with experimental results.

Still, there are many improvements that can further contribute to the model accuracy. A uniform temperature is imposed throughout. However, non-uniform heat release due to thermo-chemistry and various overpotential losses may introduce temperature non-uniformity. Note that the steam reforming is highly endothermic, and the ohmic resistance associated with ion transport through the electrolyte and the electrochemical reactions are exothermic.

Recently, it was reported that adding an interlayer between the electrode and the electrolyte improves the performance of SOFC [25]. Even though Zhao and Virkar [26] analyzed the impact of the interlayer, more work is needed to explain the role of the interlayer.

Although our anode transport and thermo-chemistry models assumed that the fuel is methane and the anode is Ni/YSZ, it was validated only for hydrogen. Using methane as a fuel, it has been observed that SOFC is rapidly deactivated due to carbon deposition on the anode because nickel in the anode catalyzes the formation of graphite from hydrocarbons and its deposition on the surface. However, almost all experimental results of SOFC using methane as a fuel were conducted while using copper in the anode material [27–30] to prevent carbon deposition. Those results with a different catalyst, copper, prevent us from validating our model applying the detailed heterogeneous kinetics of methane on the nickel surface. The detailed heterogeneous kinetics of methane on the copper surface may be valuable.

The concentrations imposed as boundary conditions at channels might be different from those in the inlet flow stream considering the flow pattern inside the button cell experiment. The inaccurate concentration boundary condition at channels might contribute to discrepancies between the model simulation results and experimental results.

Acknowledgements

Won Yong Lee wishes to acknowledge the support of the Samsung Scholarship. The work was also supported by a grant from the MIT School of Engineering.

References

[1] R.E. Williford, L.A. Chick, G.D. Maupin, S.P. Simner, J.W. Stevenson, Journal of the Electrochemical Society 150 (2003) 1067–1072.
[2] R.J. Kee, M.E. Coltrin, P. Glarborg, Chemically Reacting Flow: Theory and Practice, Wiley–Interscience, New York, 2003.
[3] E.A. Mason, A.P. Malinauskas, Gas Transport in Porous Media: The Dusty-gas Model, Elsevier, New York/Amsterdam, 1983.
[4] R. Krishna, J.A. Wesselingh, Chemical Engineering Science 52 (1997) 861–911.
[5] R.B. Bird, W.E. Stewart, E.N. Lightfoot, Transport Phenomena, 2nd ed., John Wiley & Sons Inc., New York, 2002.
[6] J. Bear, Dynamics of Fluids in Porous Media, American Elsevier Pub. Co., New York, 1972.
[7] Y. Jiang, A.V. Virkar, Journal of the Electrochemical Society 150 (2003) 942–951.
[8] W. Lehnert, J. Meusinger, F. Thom, Journal of Power Sources 87 (2000) 57–63.
[9] H. Zhu, R.J. Kee, V.M. Janardhanan, O. Deutschmann, D.G. Goodwin, Journal of the Electrochemical Society 152 (2005) 2427–2440.
[10] E.S. Hecht, G.K. Gupta, H. Zhu, A.M. Dean, R.J. Kee, L. Maier, O. Deutschmann, Applied Catalysis A: General 295 (2005) 40–51.

[11] W.Y. Lee, Modeling of solid oxide fuel cells, Master of Science, Department of Mechanical Engineering, Massachusetts Institute of Technology, Cambridge, 2006, p. 110.
[12] H. Zhu, R.J. Kee, Journal of Power Sources 117 (2003) 61–74.
[13] S.H. Chan, K.A. Khor, Z.T. Xia, Journal of Power Sources 93 (2001) 130–140.
[14] B. de Boer, SOFC anode: hydrogen oxidation at porous nickel and nickel/yttria-stabilized zirconia cermet electrodes, Ph.D., University of Twente, Netherlands, 1998.
[15] H.Z. Robert, J. Kee, David G. Goodwin, Proceedings of the Combustion Institute, 2005, pp. 2379–2404.
[16] J. Mizusaki, H. Tagawa, T. Saito, T. Yamamura, K. Kamitani, K. Hirano, S. Ehara, T. Takagi, T. Hikita, M. Ippommatsu, S. Nakagawa, K. Hashimoto, Solid State Ionics 70/71 (1994) 52–58.
[17] J.R. Wilson, W. Kobsiriphat, R. Mendoza, H.-Y. Chen, J.M. Hiller, D.J. Miller, K. Thornton, P.W. Voorhees, S.B. Adler, S.A. Barnett, Nature Materials 5 (2006) 541–544.
[18] F.H. van Heuveln, H.J.M. Bouwmeester, F.P.F. van Berkel, Journal of the Electrochemical Society 144 (1997) 126–133.
[19] M. Brown, S. Primdahl, M. Mogensen, Journal of the Electrochemical Society 147 (2000) 475–485.
[20] O. Deutschmann, S. Tischer, S. Kleditzsch, V. Janardhanan, C. Correa, D. Chatterjee, N. Mladenov, H.D. Minh, DETCHEM User Manuel, Version 2.0, Germany, 2005, http://www.detchem.com.
[21] A. Bieberle, L.P. Meier, L.J. Gauckler, Journal of the Electrochemical Society 148 (2001) A646–A656.
[22] Y. Matsuzaki, I. Yasuda, Solid State Ionics 126 (1999) 307–313.
[23] K. Sasaki, J. Maier, Solid State Ionics 134 (2000) 303–321.
[24] S.M. Haile, Acta Materialia 51 (2003) 5981–6000.
[25] T. Tsai, S.A. Barnett, Solid State Ionics 98 (1997) 191–196.
[26] F. Zhao, A.V. Virkar, Journal of Power Sources 141 (2005) 79–95.
[27] R.J. Gorte, H. Kim, J.M. Vohs, Novel SOFC anodes for the direct electrochemical oxidation of hydrocarbon, Journal of Power Sources 106 (1–2) (2002) 10–15.
[28] R.J. Gorte, S. Park, J.M. Vohs, C. Wang, Advanced Materials 12 (2000) 1465–1469.
[29] C. Lu, S. An, W.L. Worrell, J.M. Vohs, R.J. Gorte, Development of intermediate-temperature solid oxide fuel cells for direct utilization of hydrocarbon fuels, Solid State Ionics 175 (1–4) (2004) 47–50.
[30] S. Park, R. Craciun, J.M. Vohs, R.J. Gorte, Journal of the Electrochemical Society 146 (1999) 3603–3605.